COMETARY SCIENCE

Dust measurements in the coma of comet 67P/Churyumov-Gerasimenko inbound to the Sun

Alessandra Rotundi,[1,2]* Holger Sierks,[3] Vincenzo Della Corte,[1] Marco Fulle,[4] Pedro J. Gutierrez,[5] Luisa Lara,[5] Cesare Barbieri,[6] Philippe L. Lamy,[7] Rafael Rodrigo,[8,9] Detlef Koschny,[10] Hans Rickman,[11,12] Horst Uwe Keller,[13] José J. López-Moreno,[5] Mario Accolla,[1,2] Jessica Agarwal,[3] Michael F. A'Hearn,[14] Nicolas Altobelli,[15] Francesco Angrilli,[16] M. Antonietta Barucci,[17] Jean-Loup Bertaux,[18] Ivano Bertini,[19] Dennis Bodewits,[14] Ezio Bussoletti,[2] Luigi Colangeli,[20] Massimo Cosi,[21] Gabriele Cremonese,[22] Jean-Francois Crifo,[18] Vania Da Deppo,[23] Björn Davidsson,[11] Stefano Debei,[16] Mariolino De Cecco,[24] Francesca Esposito,[25] Marco Ferrari,[1,2] Sonia Fornasier,[17] Frank Giovane,[26] Bo Gustafson,[27] Simon F. Green,[28] Olivier Groussin,[7] Eberhard Grün,[29] Carsten Güttler,[3] Miguel L. Herranz,[5] Stubbe F. Hviid,[30] Wing Ip,[31] Stavro Ivanovski,[1] José M. Jerónimo,[5] Laurent Jorda,[7] Joerg Knollenberg,[30] Rainer Kramm,[3] Ekkehard Kührt,[30] Michael Küppers,[15] Monica Lazzarin,[6] Mark R. Leese,[28] Antonio C. López-Jiménez,[5] Francesca Lucarelli,[2] Stephen C. Lowry,[32] Francesco Marzari,[33] Elena Mazzotta Epifani,[25] J. Anthony M. McDonnell,[28,32,34] Vito Mennella,[25] Harald Michalik,[35] Antonio Molina,[36] Rafael Morales,[5] Fernando Moreno,[5] Stefano Mottola,[30] Giampiero Naletto,[37] Nilda Oklay,[3] José L. Ortiz,[5] Ernesto Palomba,[1] Pasquale Palumbo,[1,2] Jean-Marie Perrin,[18,38] Julio Rodríguez,[5] Lola Sabau,[39] Colin Snodgrass,[3,28] Roberto Sordini,[1] Nicolas Thomas,[40] Cecilia Tubiana,[3] Jean-Baptiste Vincent,[3] Paul Weissman,[41] Klaus-Peter Wenzel,[10] Vladimir Zakharov,[17] John C. Zarnecki[9,28]

Critical measurements for understanding accretion and the dust/gas ratio in the solar nebula, where planets were forming 4.5 billion years ago, are being obtained by the GIADA (Grain Impact Analyser and Dust Accumulator) experiment on the European Space Agency's Rosetta spacecraft orbiting comet 67P/Churyumov-Gerasimenko. Between 3.6 and 3.4 astronomical units inbound, GIADA and OSIRIS (Optical, Spectroscopic, and Infrared Remote Imaging System) detected 35 outflowing grains of mass 10^{-10} to 10^{-7} kilograms, and 48 grains of mass 10^{-5} to 10^{-2} kilograms, respectively. Combined with gas data from the MIRO (Microwave Instrument for the Rosetta Orbiter) and ROSINA (Rosetta Orbiter Spectrometer for Ion and Neutral Analysis) instruments, we find a dust/gas mass ratio of 4 ± 2 averaged over the sunlit nucleus surface. A cloud of larger grains also encircles the nucleus in bound orbits from the previous perihelion. The largest orbiting clumps are meter-sized, confirming the dust/gas ratio of 3 inferred at perihelion from models of dust comae and trails.

Although accurate measurements of the gas loss rate from comets are possible under favorable conditions even from Earth, estimates of the dust loss rate have been more uncertain thus far. Multiparametric models are needed to extract global dust parameters from the dust features of comets (coma, tail, and trail) observed from the ground and Earth-orbiting telescopes, and it is often difficult to establish the uniqueness of these model results. Past space missions had onboard instruments devoted to the measurement of the dust flux. Because all of these missions were fast flybys, it was impossible to disentangle the dust grains coming directly from the nucleus from those reflected back by solar radiation pressure (*1*, *2*). The latter component could explain part of the excess of millimeter-sized particles, showing as a bulge of the size distribution above the fitting power law derived by the observations performed during flybys at 1P/Halley (*3*) and at short-period comets 26P/Grigg-Skjellerup, 81P/Wild 2, and 9P/Tempel 1 (*4*–*6*).

An even more severe bias could affect all estimates of dust/gas ratio obtained so far in comets. The dust/gas ratio measured in 1P/Halley was close to 2 (*5*), but this number is valid up to the largest mass of ~1 g observed by the DIDSY (Dust Impact Detection System) detector (actually, this largest-mass grain was invoked to explain the spacecraft precession-inducing impact that occurred just before closest approach). Theoretical models predict that 1P/Halley was then ejecting larger masses, and the dust/gas ratio strongly depends on the actual largest grain ejected in the coma. Because it was impossible to fix the size distribution between 1 g and the unknown largest ejected mass, we cannot exclude dust/gas values a factor of 10 higher. In this paper, we show that for comet 67P/Churyumov-Gerasimenko (67P hereafter), we can disentangle the two families of ejected grains (direct and reflected) and extract the dust size distribution up to the largest ejected grain, obtaining for the first time an accurate estimate of the dust/gas ratio.

[1]Istituto di Astrofisica e Planetologia Spaziali, Istituto Nazionale di Astrofisica (INAF), Via Fosso del Cavaliere, 100, 0133 Rome, Italy. [2]Università degli Studi di Napoli "Parthenope," Dipartimento di Scienze e Tecnologie, CDN IC4, 80143 Naples, Italy. [3]Max-Planck-Institut für Sonnensystemforschung, Justus-von-Liebig-Weg, 3, 37077 Göttingen, Germany. [4]Osservatorio Astronomico, INAF, Via Tiepolo 11, 34143 Trieste, Italy. [5]Instituto de Astrofísica de Andalucía, Consejo Superior de Investigaciones Científicas (CSIC), P.O. Box 3008, 18080 Granada, Spain. [6]Department of Physics and Astronomy, Padova University, Vicolo dell'Osservatorio 3, 35122 Padova, Italy. [7]Laboratoire d'Astrophysique de Marseille, UMR 7326, CNRS and Aix-Marseille Université, 13388 Marseille, France. [8]Centro de Astrobiologia (Instituto Nacional de Tecnica Aerospacial–CSIC), 28691 Villanueva de la Canada, Madrid, Spain. [9]International Space Science Institute, Hallerstrasse 6, CH-3012 Bern, Switzerland. [10]Scientific Support Office, European Space Agency, 2201 Noordwijk, Netherlands. [11]Department of Physics and Astronomy, Uppsala University, Box 516, 75120 Uppsala, Sweden. [12]Polish Academy of Sciences Space Research Center, Bartycka 18A, PL-00716 Warszawa, Poland. [13]Institute for Geophysics and Extraterrestrial Physics, Technische Universität Braunschweig, Braunschweig 38106, Germany. [14]Department of Astronomy, University of Maryland, College Park, MD 20742-2421, USA. [15]European Space Agency (ESA)–European Space Astronomy Center (ESAC), Camino Bajo del Castillo, s/n, 28692 Villanueva de la Cañada, Madrid, Spagna. [16]Department of Mechanical Engineering, University of Padova, via Venezia 1, 35131 Padova, Italy. [17]Laboratoire d'Etudes Spatiales et d'Instrumentation en Astrophysique, Observatoire de Paris, CNRS, Université Paris 06, Université Paris-Diderot, 5 place Johannes Janssen, 92195 Meudon, France. [18]Laboratoire Atmosphères, Milieux, Observations Spatiales, CNRS/Université de Versailles Saint-Quentin-en-Yvelines/Institut Pierre-Simon Laplace, 11 boulevard d'Alembert, 78280 Guyancourt, France. [19]University of Padova, Centro Interdipartimentale di Studi e Attività Spaziali (CISAS), via Venezia 15, 35100 Padova, Italy. [20]ESA, European Space Research and Technology Centre (ESTEC), Keplerlaan 1, 2201 AZ Noordwijk, Netherlands. [21]Selex-ES, Via Albert Einstein, 35, 50013 Campi Bisenzio, Firenze, Italy. [22]Osservatorio Astronomico di Padova, INAF, Vicolo dell'Osservatorio 5, 35122 Padova, Italy. [23]Consiglio Nazionale delle Ricerche–Istituto di Fotonica e Nanotecnologie–Unità Operativa di Supporto Padova LUXOR, via Trasea 7, 35131 Padova, Italy. [24]Università di Trento, via Mesiano, 77, 38100 Trento, Italy. [25]Osservatorio Astronomico di Capodimonte, INAF, Salita Moiariello, 16, 80133 Naples, Italy. [26]Virginia Polytechnic Institute and State University, Blacksburg, VA 24061, USA. [27]University of Florida, Gainesville, FL 32611, USA. [28]Planetary and Space Sciences, Department of Physical Sciences, The Open University, Milton Keynes MK7 6AA, UK. [29]Max-Planck-Institut fuer Kernphysik, Saupfercheckweg 1, 69117 Heidelberg, Germany. [30]Institute of Planetary Research, Deutsches Zentrum für Luft- und Raumfahrt (DLR), Rutherfordstrasse 2, 12489 Berlin, Germany. [31]Institute for Space Science, National Central University, 300 Chung Da Road, 32054 Chung-Li, Taiwan. [32]The University of Kent, School of Physical Sciences, Canterbury, Kent CT2 7NZ, UK. [33]Department of Physics, University of Padova, 35131 Padova, Italy. [34]Unispacekent, Canterbury CT2 8EF, UK. [35]Institut für Datentechnik und Kommunikationsnetze, 38106 Braunschweig, Germany. [36]Departamento de Física Aplicada, Universidad de Granada, Facultad de Ciencias, Avenida Severo Ochoa, s/n, 18071 Granada, Spain. [37]Department of Information Engineering, Padova University, via Gradenigo 6, 35131 Padova, Italy. [38]Observatoire de Haute Provence OSU Pythéas UMS 2244 CNRS-AMU, 04870 Saint Michel l'Observatoire, France. [39]Instituto Nacional de Tecnica Aeroespacial, Carretera de Ajalvir, p.k. 4, 28850 Torrejon de Ardoz, Madrid, Spain. [40]Physikalisches Institut, Sidlerstrasse 5, University of Bern, 3012 Bern, Switzerland. [41]Planetary Science Section, Jet Propulsion Laboratory, 4800 Oak Grove Drive, Pasadena, CA 91109, USA.
***Corresponding author. E-mail: rotundi@uniparthenope.it**

OSIRIS (Optical, Spectroscopic, and Infrared Remote Imaging System) (*7*) has detected a dust coma since an outburst that occurred between 27 and 30 April 2014, and possibly since the first images taken on 23 March (*8*). We started to detect coma features in long wide-angle camera (WAC) exposures at the end of July 2014 at 3.7 astronomical units (AU) from the Sun. Most of the activity was coming out of the transition region between the small and large lobes of the nucleus, the Hapi region (*9*). This major coma feature showed a diurnal variation of intensity, and its brightness contribution was measured in WAC images taken on 10 August 2014 at 110 km from the nucleus. This single jet-like feature contributed roughly 10% of the total dust brightness: Such a dominance is rare among active comets closer to the Sun but may be true for activity as it first turns on. The background dust brightness may come from smaller features and/or isotropic emission from the nucleus surface.

GIADA (Grain Impact Analyzer and Dust Accumulator) consists of three subsystems: (i) the grain-detection system (GDS) to detect dust grains as they pass through a laser curtain; (ii) the impact sensor (IS) to measure grain momentum derived from the impact on a plate connected to five piezoelectric sensors; and (iii) the microbalances system (MBS), five quartz crystal microbalances in roughly orthogonal directions providing the cumulative dust flux of grains smaller than 10 μm. GDS provides data on grain speed and its optical cross section. The IS momentum measurement, when combined with the GDS detection time, provides a direct measurement of grain speed and mass (*10*, *11*). Using these combined measurements, we are able to characterize the dynamics of single grains.

GIADA began operating in continuous mode on 18 July 2014 when the comet was at a heliocentric distance of 3.7 AU. The first grain detection occurred when the spacecraft was 814 km from the nucleus on 1 August 2014. Three additional grains were detected at distances of 603, 286, and 179 km from the nucleus during the spacecraft approach. Once in orbit about the nucleus, 19 impacts were recorded by the IS at distances ranging from 90 to 30 km, while during the same period GDS detected seven particles. A total of nine combined GDS+IS events (i.e., measured by both the GDS and IS detectors) allow us to extract the complete set of dust grain parameters: mass, speed, velocity vector, and optical cross section. From these GDS+IS detections, we combined the measured optical cross sections (GDS) with the momenta (IS) to constrain the bulk density range to $(1.9 \pm 1.1) \times 10^3$ kg m^{-3}, assuming spherical grains (i.e., the lowest cross section/mass ratio). Grain cross sections (Table 1) are retrieved by means of two GIADA calibration

Table 1. GIADA GDS+IS detections made at heliocentric distances between 3.6 and 3.4 AU. The grain momentum and speed (v) are direct GIADA measurements from which the mass (m) is calculated. Grain geometrical cross sections are derived by the GDS calibration curves obtained with amorphous carbon and with a mixture of alkali-feldspar, melilite, and anorthite grains. R is the detection distance from the nucleus. The IS-sensitive area* is 10^{-2} m^2. Q_m is the dust mass loss rate per grain. The error of the velocity measurements is 6%.

Event no.	Date [dd/mm/yyyy]	Momentum [kg m s^{-1}]	v [m s^{-1}]	m [kg]	Cross section [m^2]	R [km]	Q_m [kg s^{-1}]
5	11/08/2014	$3.1 \pm 1.3 \times 10^{-8}$	3.2	$9.8 \pm 4.0 \times 10^{-9}$	$5.6 \pm 1.9 \times 10^{-8}$	92.9	1.9×10^{-2}
16	23/08/2014	$2.1 \pm 0.8 \times 10^{-7}$	2.6	$8.0 \pm 3.2 \times 10^{-8}$	$1.4 \pm 0.4 \times 10^{-7}$	61.7	6.8×10^{-2}
21	29/08/2014	$2.3 \pm 0.9 \times 10^{-8}$	4.7	$4.9 \pm 2.0 \times 10^{-9}$	$2.3 \pm 1.2 \times 10^{-8}$	54.0	3.2×10^{-3}
23	30/08/2014	$2.0 \pm 0.8 \times 10^{-7}$	2.6	$7.8 \pm 3.2 \times 10^{-8}$	$9.2 \pm 3.0 \times 10^{-8}$	57.4	5.8×10^{-2}
26	01/09/2014	$2.0 \pm 0.8 \times 10^{-8}$	2.9	$6.9 \pm 2.9 \times 10^{-9}$	$2.7 \pm 1.9 \times 10^{-8}$	53.2	4.4×10^{-3}
27	01/09/2014	$3.9 \pm 1.6 \times 10^{-8}$	2.8	$1.4 \pm 0.5 \times 10^{-8}$	$7.4 \pm 2.3 \times 10^{-8}$	51.8	8.4×10^{-3}
33	12/09/2014	$1.6 \pm 1.0 \times 10^{-9}$	3.0	$5.3 \pm 3.3 \times 10^{-10}$	$3.1 \pm 0.3 \times 10^{-8}$	29.7	2.1×10^{-3}*
34	12/09/2014	$1.3 \pm 0.5 \times 10^{-7}$	2.8	$4.6 \pm 1.9 \times 10^{-8}$	$7.4 \pm 0.6 \times 10^{-8}$	29.7	9.1×10^{-3}
35	13/09/2014	$8.3 \pm 3.7 \times 10^{-9}$	3.6	$2.3 \pm 1.0 \times 10^{-9}$	$3.1 \pm 1.6 \times 10^{-8}$	30.1	4.7×10^{-4}

*For momentum values close to the IS detection limit (6.5×10^{-10} kg m s^{-1}), a correction factor to the IS-sensitive area has to be taken into account; e.g., only 30% of the total IS-sensitive area has a sufficient sensitivity to detect values of momentum as small as 2.5×10^{-9} kg m s^{-1}. For the grain density estimate, this detection was not taken into account because the derived density was far off the density of all the materials used to retrieve the calibration curves.

Table 2. Impacts on GIADA, detected by IS only, from 3.6 to 3.4 AU. Dust speed is assumed from (*18*) for a dust bulk density of 1×10^3 (grain a) and 3×10^3 kg m^{-3} (grain b). The IS-sensitive area* is 10^{-2} m^2.

Event no.	Date [dd/mm/yyyy]	Momentum [kg m s^{-1}]	A [m^2]	v (a) [m s^{-1}]	v (b) [m s^{-1}]	m (a) [kg]	m (b) [kg]	R [km]	Q_m (a) [kg s^{-1}]	Q_m (b) [kg s^{-1}]
9	11/08/2014	$1.8 \pm 1.6 \times 10^{-9}$	8.0×10^{-4}	10.0	6.6	1.8×10^{-10}	2.7×10^{-10}	92.9	4.4×10^{-3}	6.5×10^{-3}
10	11/08/2014	$1.2 \pm 0.5 \times 10^{-8}$	1.0×10^{-2}	6.6	4.7	1.8×10^{-9}	2.6×10^{-9}	91.1	3.4×10^{-3}	4.8×10^{-3}
11	12/08/2014	$2.2 \pm 1.7 \times 10^{-9}$	2.0×10^{-3}	10.0	6.6	2.2×10^{-10}	3.3×10^{-10}	93.9	2.2×10^{-3}	3.3×10^{-3}
12	15/08/2014	$5.3 \pm 2.1 \times 10^{-8}$	1.0×10^{-2}	4.7	3.2	1.1×10^{-8}	1.7×10^{-8}	92.3	2.1×10^{-2}	3.2×10^{-2}
13	19/08/2014	$2.8 \pm 1.1 \times 10^{-8}$	1.0×10^{-2}	6.6	4.7	4.2×10^{-9}	6.0×10^{-9}	78.9	5.9×10^{-3}	8.4×10^{-3}
14	22/08/2014	$1.4 \pm 0.6 \times 10^{-8}$	1.0×10^{-2}	6.6	4.7	2.2×10^{-9}	3.0×10^{-9}	63.4	2.0×10^{-3}	2.7×10^{-3}
17	26/08/2014	$2.5 \pm 1.9 \times 10^{-9}$	3.0×10^{-3}	10.0	6.6	2.5×10^{-10}	3.8×10^{-10}	55.0	5.7×10^{-4}	8.6×10^{-4}
18	26/08/2014	$6.6 \pm 3.1 \times 10^{-9}$	9.8×10^{-3}	6.6	4.7	1.0×10^{-9}	1.4×10^{-9}	61.9	8.8×10^{-4}	1.2×10^{-3}
19	29/08/2014	$1.8 \pm 0.8 \times 10^{-8}$	1.0×10^{-2}	6.6	4.7	2.7×10^{-9}	3.8×10^{-9}	53.7	1.7×10^{-3}	2.5×10^{-3}
20	29/08/2014	$6.2 \pm 3.0 \times 10^{-9}$	9.7×10^{-3}	6.6	4.7	9.4×10^{-10}	1.3×10^{-9}	53.8	6.3×10^{-4}	8.7×10^{-4}
22	30/08/2014	$9.4 \pm 4.1 \times 10^{-9}$	1.0×10^{-2}	6.6	4.7	1.4×10^{-9}	2.0×10^{-9}	56.0	9.8×10^{-4}	1.4×10^{-3}
24	30/08/2014	$1.2 \pm 0.5 \times 10^{-8}$	1.0×10^{-2}	6.6	4.7	1.8×10^{-9}	2.6×10^{-9}	58.6	1.4×10^{-3}	2.0×10^{-3}
28	02/09/2014	$2.0 \pm 0.8 \times 10^{-8}$	1.0×10^{-2}	6.6	4.7	3.0×10^{-9}	4.3×10^{-9}	54.2	2.0×10^{-3}	2.8×10^{-3}
30	09/09/2014	$1.1 \pm 0.4 \times 10^{-7}$	1.0×10^{-2}	4.7	3.2	2.3×10^{-8}	3.4×10^{-8}	29.3	4.4×10^{-3}	6.5×10^{-3}
31	09/09/2014	$9.6 \pm 4.2 \times 10^{-9}$	1.0×10^{-2}	6.6	4.7	1.5×10^{-9}	2.0×10^{-9}	29.2	2.9×10^{-4}	3.8×10^{-4}

*For momentum values close to the IS detection limit (6.5×10^{-10} kg m s^{-1}), a correction factor to the IS-sensitive area has to be taken into account; e.g., only 30% of the total IS-sensitive area has a sufficient sensitivity to detect values of momentum as small as 2.5×10^{-9} kg m s^{-1}, and only 8% has a sufficient sensitivity to detect values of momentum as small as 1.8×10^{-9} kg m s^{-1}.

curves, GDS signal versus the grain measured geometrical cross section, obtained using grains of amorphous carbon and grains of a mixture of alkali-feldspar, melilite, and anorthite to get the extreme cases of dark and bright materials. The GIADA estimates of grain bulk densities fit the range of the measured bulk densities of interplanetary dust particles, some of which have cometary origins and sizes comparable to the grains detected by GIADA (*12*). They are also compatible with those inferred for the collected comet 81P/Wild 2 particles (*13*). The Stardust mission caused a dramatic paradigm shift in our understanding of the transport of debris from the evolving asteroid belt to the heliocentric distances of the present-day Kuiper belt (*14*). It was found that the minerals, chondrule fragments, and calcium-aluminum–rich inclusions in comet 81P/Wild 2 dust have their counterparts in chondritic meteorites (*15*), which is confirmed by the still ongoing laboratory analyses of Wild 2 samples (*16*).

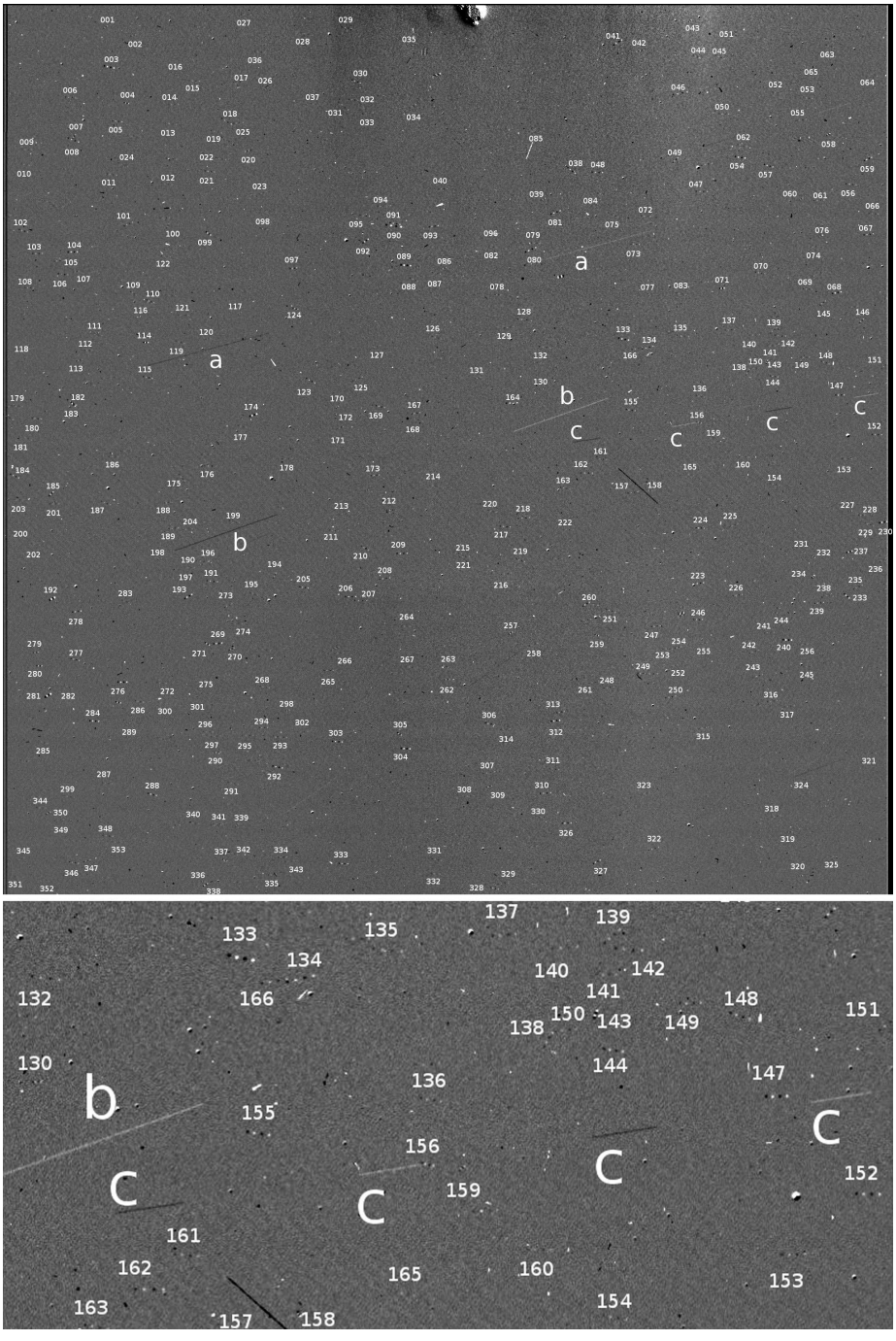

Fig. 1. Detections of single grains by OSIRIS. (**Top**) Bound grains detected in the first set of NAC images (each labeled by a number from 001 to 353) and the brightest three tracks of the 48 outflowing grains (each labeled by letters a, b, and c). The 67P nucleus is visible at the top of the panel. (**Bottom**) Zoom centered on track c. The images were shifted to align stars on the same pixels. The spacecraft motion is to the right, with an angle of 6° counterclockwise from the +x image axis. Grain c shows all of the expected four white and black tracks; grains a and b have two tracks outside the image. The detections of bound grains (white-black-white-black dots) show a uniform space distribution. Further details and explanations are available in the supplementary materials.

To extract the dust/gas mass ratio from our data, we compare our estimated dust mass loss rates to the water production rate measured by the MIRO (Microwave Instrument for the Rosetta Orbiter) instrument on board Rosetta [1.2 kg s^{-1} at 3.5 AU with diurnal variations of 50% (*17*)]. MIRO adopted a hemispherical gas ejection model from the nucleus surface. To retrieve a meaningful dust/gas ratio, we assume the same hemispherical dust ejection. If both gases and dust are ejected within a smaller solid angle, we will overestimate both the gas and the dust mass loss rates, but we will still obtain the correct dust/gas mass ratio. We discuss the dust size distribution between 3.6 and 3.4 AU. Table 1 lists the nine GDS+IS events with measured momentum and speed from which we can calculate the grain mass (m) directly. We compute the derived mass loss rate per grain at the nucleus

$$Q_m = 2\pi m R^2 (A\Delta t)^{-1} \quad (1)$$

where $\Delta t = 2.8 \times 10^6$ s is the collection time, R is the distance of the spacecraft from the nucleus center of mass, and A is the effective IS collecting area. Because the spacecraft radial velocity (always lower than 0.1 m s^{-1}) is much smaller than the dust velocity, the conversion from observed impacts to dust loss rate at the nucleus does not depend on the dust velocity. Table 2 completes the list of IS detections. The grain momentum is measured but not the speed. The grain speed (v) is therefore derived from a model applied to ground-based observations of 67P at 3.2 AU (*18*), for two assumed bulk densities of 1×10^3 kg m^{-3} (for grain a) and 3×10^3 kg m^{-3} (for grain b). The nine dust velocities measured by the GDS+IS match the predictions by Fulle *et al.* (*18*) at 3.2 AU very well for a dust bulk density of 3×10^3 kg m^{-3}. We cannot exclude higher dust velocities

Table 3. Radial velocity distribution in the comet reference frame of the 48 outflowing grains detected by OSIRIS.

Velocity bin (m s^{-1})	Number of grains
0–1	2
1–2	10
2–3	5
3–4	9
4–5	7
5–6	1
6–7	2
7–8	4
8–9	3
>9	5

at lower dust masses and bulk densities, as predicted by all models of dust drag by gas.

To complement the GIADA data and to estimate the largest dust mass ejected from 67P, we consider the detections of single grains by the OSIRIS narrow-angle camera (NAC) (*7*) on 4 August 2014 at a distance of 3.6 AU from the Sun and 275 km from the nucleus (Fig. 1). These observations allowed us to detect ~350 grains in bound orbits around the comet nucleus and 48 fast and outflowing grains that were ejected about a day before the observations and had diameters up to 17 mm (see details in the supplementary materials). We compute the velocity of the outflowing grains assuming that the grain motion is strictly radial from the nucleus. The velocity distribution in the nucleus reference frame is shown in Table 3. The wide distribution is also due to a nonperfectly radial velocity of the grains, because a grain proper transverse speed of 0.18 m s^{-1} changes the extracted radial velocity by a factor 2. Because proper transverse speeds are expected to be random, averages of the extracted radial velocities cancel out the effects of individual transverse speeds. We conclude that, on average, the median of the radial velocity is 3.5 m s^{-1}, in agreement with measurements of other grains by GIADA. The observed velocities do not show any evident trend with respect to the grain size.

Regarding bound grains, the radius of 67P's Hill sphere (318 km) corresponds to a coma volume of 10^{14} m^3 in NAC images, providing the observed space density of 3.5×10^{-12} m^{-3}. This value fits the space density predicted by models of bound dust clouds around comet 46P/Wirtanen (*19*), assuming a nucleus with the same mass as 67P (*9*, *19*). The predicted cloud density ranges from 5×10^{-13} m^{-3} to 2×10^{-11} m^{-3}, taking into account the difference between the dust mass loss of 46P and 67P (*18*, *19*) and a possible range of the dust bulk density from 4×10^2 kg m^{-3} (*9*) to 3×10^3 kg m^{-3} (this paper). Photometry of the bound grains provides diameters ranging from 4 cm, in agreement with dynamical constraints (*20*), to ~2 m. Models of bound grain orbits (*19*, *21*) show that an isotropic bound cloud needs years to be built up. The observed bound grains could not be ejected during the outburst observed at the end of April 2014 (*8*). They were probably put in bound orbits just after the previous perihelion, when the gas loss rate was decreasing and no longer perturbing the bound orbits (*19*). The same gas perturbations, during the current increase of the gas production rate, may dissipate the bound cloud in a few months.

The two families of detected grains (outflowing and bound) do not overlap in space. Outflowing grains are not detected farther than 20 km from the spacecraft, whereas bound grains are not detected closer than 130 km from the spacecraft. The space density of bound grains is at least 100 times lower than that of outflowing grains: Detections closer than 130 km are improbable (at most, three bound grains in a coma volume 100 times lower than up to 600 km). Taking into account the different pixel areas covered by the faintest bound (dots) and outflowing grains (tracks), the ratio of sizes between farthest outflowing and closest bound grains becomes consistent with the ratio of respective detection distances (20 versus 130 km). The track of the farthest outflowing grain is 16 NAC pixels long. This proves that, if larger and more distant young grains were outflowing in 67P's coma, they would have been easily detected. The size distribution of outflowing grains bigger than 2 cm has a large drop, probably due to the low gas density at the nucleus surface, still lifting very few larger grains at 3.6 AU. This conclusion is not affected by the possibility that some of the grains identified as bound are, in fact, outflowing. Their number and space density would be so low as to not change the cut-off of the size distribution above a diameter of 2 cm. This largest size is therefore well constrained and allows us to combine results from GIADA and OSIRIS to reach a precise measurement of the dust/gas ratio.

Tables 4 and 5 and Fig. 2 summarize our results for both OSIRIS (the three upper mass bins) and GIADA (the three lower-mass bins) and for dust bulk densities of 1×10^3 and 3×10^3 kg m^{-3}. For the GIADA detections, the dust mass loss rate per mass bin (Q_m) is the sum of all Q_m values in Tables 1 and 2. In addition, we performed a similar sum for three different subsets of Tables 1 and 2, namely dividing the total 24 samples into three sets of 8 samples each, one following the other in time. All the results were consistent (within 20%) with those shown in Tables 4 and 5. This shows that (i) the 24 samples provide a sufficient sampling for the 67P dust size distribution, and (ii) the dust mass loss rate remained approximately constant from 3.6 to 3.4 AU. Diurnal variations of the water loss rate mask any gas loss rate trend versus the heliocentric distance. For the OSIRIS detections, the dust loss rate was extracted from the dust space density ρ at the spacecraft, which was computed on coma volumes defined by the distance D from the spacecraft to the faintest (just above the detection limit) grain in each mass bin (i.e., the coma volume surveyed by the OSIRIS-NAC). N is the number of detections (for the OSIRIS data, N was divided by the number of images providing independent detections), v is the mean dust radial velocity (thus canceling out transverse speed effects), and Q_n is the number loss rate for hemispherical dust ejection

$$Q_n = 2\pi\rho v R^2 \quad (2)$$

Tables 4 and 5 and Fig. 2 show the quantity

$$Af\rho = 2A_p Q_n \sigma / v \quad (3)$$

for each mass bin, where σ is the mean dust cross section in each mass bin, and the geometric albedo A_p = 5% (*18*, *22*). $Af\rho$ provides the dust mass dominating the dust coma optical flux and shows a clear maximum at half-millimeter sizes. The total $Af\rho$ reaches 8 ± 4 cm after we fill

Table 4. GIADA and OSIRIS data on the 67P dust environment, assuming a dust bulk density of 1×10^3 kg m^{-3}. D is the distance of the grains observed (just above the detection limit) by OSIRIS-NAC to the spacecraft; N is the number of detections (for the OSIRIS data, N was divided by the number of images providing independent detections); ρ is the dust space density derived from N; v is the mean dust radial velocity (for the 48 OSIRIS detections, v has been computed assuming that the motion is radial from the nucleus); Q_n is the number loss rate for hemispherical dust ejection; Q_m is the dust mass loss rate per mass bin; and $Af\rho$ provides the dust brightness per mass bin. N/A, not applicable.

Mass bin [kg]	N	D [km]	ρ [m^{-3}]	v [m s^{-1}]	Q_n [s^{-1}]	Q_m [kg s^{-1}]	$Af\rho$ [m]
10^{-3}–10^{-2}	0.4	20	1.0×10^{-10}	7.2	3.9×10^2	0.9	1.8×10^{-3}
10^{-4}–10^{-3}	2.2	16	1.1×10^{-9}	5.7	3.9×10^3	1.2	5.0×10^{-3}
10^{-5}–10^{-4}	7	10	1.4×10^{-8}	4.4	3.6×10^4	1.5	1.3×10^{-2}
10^{-8}–10^{-7}	6	N/A	N/A	2.4	4.2×10^6	0.17	2.8×10^{-2}
10^{-9}–10^{-8}	13	N/A	N/A	4.7	1.4×10^7	4.6×10^{-2}	1.0×10^{-2}
10^{-10}–10^{-9}	5	N/A	N/A	6.9	2.4×10^7	9.9×10^{-3}	2.6×10^{-3}

Table 5. GIADA and OSIRIS data of the 67P dust environment, assuming a dust bulk density of 3×10^3 kg m^{-3}. See Table 4 for a description of parameters. N/A, not applicable.

Mass bin [kg]	N	D [km]	ρ [m^{-3}]	v [m s^{-1}]	Q_n [s^{-1}]	Q_m [kg s^{-1}]	$Af\rho$ [m]
10^{-3}–10^{-2}	1.2	20	3.0×10^{-10}	5.1	8.7×10^2	3.0	2.8×10^{-3}
10^{-4}–10^{-3}	5.2	16	2.6×10^{-9}	4.4	6.7×10^3	1.7	5.4×10^{-3}
10^{-5}–10^{-4}	3.2	10	6.4×10^{-9}	5.5	2.0×10^4	1.4	2.8×10^{-3}
10^{-8}–10^{-7}	6	N/A	N/A	1.9	4.2×10^6	0.18	1.7×10^{-2}
10^{-9}–10^{-8}	14	N/A	N/A	3.4	1.4×10^7	5.4×10^{-2}	6.8×10^{-3}
10^{-10}–10^{-9}	4	N/A	N/A	4.7	3.4×10^7	1.3×10^{-2}	2.6×10^{-3}

the gap from 10^{-7} to 10^{-5} kg with the observed lowest and largest $Af\rho$ values, respectively. Ground-based observations provided $Af\rho$ = 7 cm when the comet was at 5 AU, and $Af\rho$ = 20 cm at 3.4 AU inbound (*22*). Q_m is approximately constant at larger-than-millimeter sizes, suggesting a differential size distribution power law index = −4, in agreement with (*18*, *23*). At smaller-than-millimeter sizes, Q_m drops faster than predicted by (*18*), suggesting a shallower differential size distribution, with a power law index close to −2. The same model (*18*) predicts a MBS response 10 times higher than the MBS sensitivity. However, the MBS signal at these 67P heliocentric distances did not reach the minimum sensitivity level, suggesting no measurable accumulation of dust grains smaller than 10^{-11} kg and confirming that the power law index of the differential size distribution is close to −2 over the entire size spectrum, from submicrometer grains up to 10^{-7} kg. Assuming this size distribution (power index close to −2), the MBS flux becomes lower than the sensitivity limit, and $Af\rho$ has a sharp maximum at the upper mass; i.e., at 10^{-7} kg, as shown in Fig. 2. The number of micrometer-sized grains in 67P is too low to provide any substantial optical scattering with respect to that coming from millimeter-sized grains, a fact never confirmed before in any comet. The $Af\rho$ value observed at 3.4 AU (*22*), which is larger than our value of 8 ± 4 cm, may be explained by (i) larger $Af\rho$ values from 10^{-7} to 10^{-5} kg, (ii) a larger σ due to non-spherical dust shape, and (iii) A_p > 5%. Comet 67P's dust loss rate from 3.6 to 3.4 AU of 7 ± 1 kg s^{-1}, derived by interpolation between the GIADA and OSIRIS data to fill the gap from 10^{-7} to 10^{-5} kg, is consistent with an average of predicted dust loss rates at 3.2 AU [column for 3.2 AU in tables 3 and 4 of (*18*)].

Taking into account the MIRO measurements of the water production rate and the results obtained by the Rodionov-Zakharov-Crifo (RZC) coma model (*24*), applied to 67P to forecast the lander descent environment, the derived dust/gas mass ratio is 6 ± 2 for water only. The RZC model fits ROSINA-COPS (Rosetta Orbiter Spectrometer for Ion and Neutral Analysis–Comet Pressure Sensor) data, assuming the out-flow of water and of other gases in proportion to the local illumination. The obtained water loss rate fits that directly provided by MIRO data within the diurnal oscillations. Computations are ongoing to further constrain the whole three-dimensional and time-dependent coma by means of other Rosetta data. The dust/gas mass ratio decreases to 4 ± 2 if we use a total gas loss rate that includes CO and CO_2 [~50% in mass with respect to water according to ROSINA data (*25*)]. An estimated dust/gas ratio of 3 for 67P at perihelion was predicted assuming that meter-sized clumps are ejected at perihelion (*15*). This assumption is supported by the observations of the bound cloud of grains observed by OSIRIS-NAC. The dust number loss rate (Q_n) shows a systematic increase from the largest to the smallest measured dust masses, as is expected in a power law distribution. This is true also at the lowest mass bin measured by GIADA, showing that the effective IS collecting area (A) in Tables 1 and 2 compensates the bias of the low number of grain detections (N), due to the momentum sensitivity limit, in this mass bin. Therefore, the Q_m and $Af\rho$ values in the lowest mass bin (Table 3 and Fig. 2), should be considered a good estimate of the real values. The very good match of the two size distributions obtained by two independent instruments and techniques (in situ dust collection by GIADA versus remote optical detection by OSIRIS) suggests that the same dust bulk density range estimated from the GIADA data is a good assumption also for the single grains detected by OSIRIS.

In conclusion, at heliocentric distances between 3.7 and 3.4 AU: (i) GIADA on Rosetta is working well in characterizing the dust flux and, in particular, for carrying out measurements including dust grain speed, momentum, mass, and optical cross section and furthermore constraining derived values of the grain bulk densities. (ii) The dust/gas mass ratio, averaged over the sunlit nucleus surface, is 4 ± 2 but may change as the comet approaches closer to the Sun. The estimate of the diameter of the largest clumps in a bound cloud (probably built-up just after the previous perihelion passage) confirms the dust/gas ratio of 3 inferred at perihelion (*18*). (iii) The dust optical scattering is dominated by 100-μm to millimeter-sized grains, not by micrometer-sized grains [this is expected to change approaching to perihelion (*18*)]. (iv) The GIADA dust model predictions at 3.2 AU (*18*) are consistent with the measured data. (v) The detection by OSIRIS-NAC of a cloud of grains in bound orbits confirms predictions of its density (*19*) and sizes of the orbiting grains (*20*).

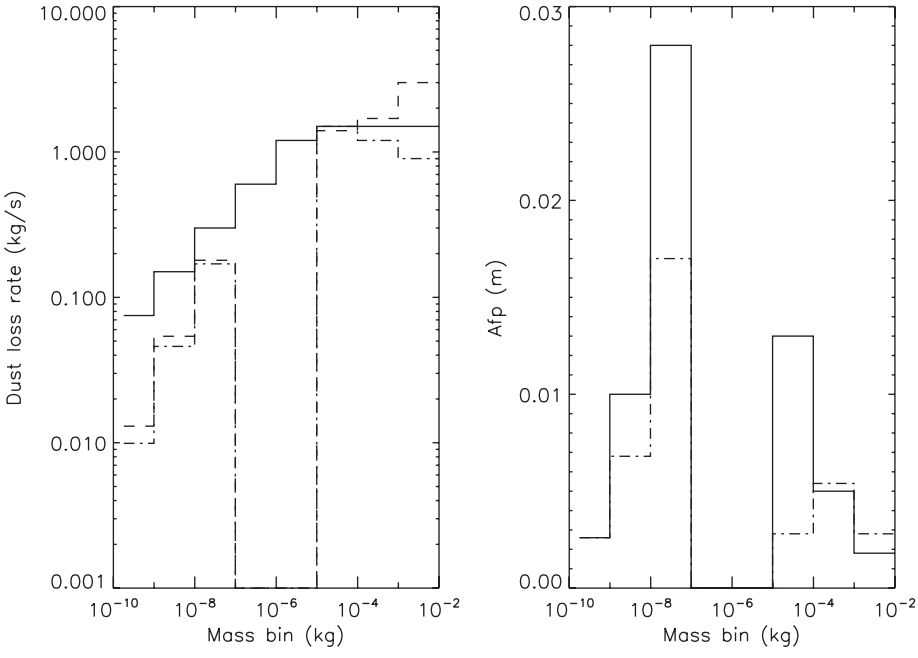

Fig. 2. 67P grain mass distribution. (**Left**) Mass distribution of 67P dust grains as measured by GIADA and OSIRIS. Dot-dashed line: dust loss rate by GIADA (three lower-mass bins) and OSIRIS (three higher-mass bins) at bulk density 1×10^3 kg m^{-3}. Dashed line: dust loss rate by GIADA (three lower-mass bins) and OSIRIS (three higher-mass bins) at bulk density 3×10^3 kg m^{-3}. Both the mass distributions have differential size distribution power law indices close to −2 in the three lower-mass bins. Solid line: average dust loss rate predicted by (*18*) at 3.2 AU. Differential size distribution power index = −4 in the three higher-mass bins and −3 elsewhere. (**Right**) Solid line: dust coma brightness-equivalent size $Af\rho$ derived from GIADA (three lower-mass bins) and OSIRIS (three higher-mass bins) data with bulk density 1×10^3 kg m^{-3}. Dot-dashed line: $Af\rho$ derived from GIADA (three lower-mass bins) and OSIRIS (three higher-mass bins) data with bulk density 3×10^3 kg m^{-3}. Both of these distributions have a clear maximum in the 10^{-8}- to 10^{-7}-kg mass bin, corresponding to a size of hundreds of micrometers.

REFERENCES AND NOTES

1. M. Fulle, L. Colangeli, V. Mennella, A. Rotundi, E. Bussoletti, The sensitivity of the size distribution to the grain dynamics: Simulation of the dust flux measured by GIOTTO at P/Halley. *Astron. Astrophys.* **304**, 622–630 (1995).
2. M. Fulle, A. C. Levasseur-Regourd, N. McBride, E. Hadamcik, In situ dust measurements from within the coma of 1P/Halley: First-order approximation with a dust dynamical model. *Astron. J.* **119**, 1968–1977 (2000). doi: 10.1086/301285
3. J. A. M. McDonnell, G. S. Pankiewicz, P. N. W. Birchley, S. F. Green, C. H. Perry, "The comet nucleus: Ice and dust morphological balances in a production surface of comet P/Halley," in *Proceedings of the 20th Lunar and Planetary Science Conference*, 13 to 17 March 1989 (Lunar and Planetary Institute, Houston, TX, 1990), pp. 373–378.
4. J. A. M. McDonnell *et al.*, Dust particle impacts during the Giotto encounter with Comet Grigg-Skjellerup. *Nature* **362**, 732–734 (1993). doi: 10.1038/362732a0
5. S. F. Green *et al.*, The dust mass distribution of comet 81P/Wild 2. *J. Geophys. Res.* **109**, E12S04 (2004). doi: 10.1029/2004JE002318
6. T. E. Economou, S. F. Green, D. E. Brownlee, B. C. Clark, Dust flux monitor instrument measurements during Stardust-NExT flyby of comet 9P/Tempel 1. *Icarus* **222**, 526–539 (2013). doi: 10.1016/j.icarus.2012.09.019

7. H. U. Keller *et al*., OSIRIS - The scientific camera system onboard Rosetta. *Space Sci. Rev.* **128**, 433–506 (2007). doi: 10.1007/s11214-006-9128-4
8. C. Tubiana *et al*., 67P/Churyumov-Gerasimenko: Activity between March and June 2014 as observed from Rosetta/OSIRIS. *Astron. Astrophys.* **573**, A62 (2015). doi: 10.1051/0004-6361/201424735
9. H. Sierks *et al*., On the nucleus structure and activity of comet 67P/Churyumov-Gerasimenko. *Science* **347**, aaa1044 (2015). doi: 10.1126/science.aaa1044
10. V. Della Corte *et al*., GIADA: Its status after the Rosetta cruise phase and on-ground activity in support of the encounter with comet 67P/Churyumov-Gerasimenko. *J. Astron. Instrum.* **03**, 1350011 (2014). doi: 10.1142/S2251171713500116
11. L. Colangeli *et al*., The Grain Impact Analyser and Dust Accumulator (GIADA) experiment for the Rosetta mission: Design, performances and first results. *Space Sci. Rev.* **128**, 803–821 (2007). doi: 10.1007/s11214-006-9038-5
12. F. J. M. Rietmeijer, "Interplanetary dust particles," in *Planetary Materials, Reviews in Mineralogy*, J.J. Papike, Ed. (Mineralogical Society of America, Chantilly, VA, 1998), vol. 36, pp. 2-1–2-95.
13. A. T. Kearsley *et al*., Dust from comet Wild 2: Interpreting particle size, shape, structure, and composition from impact features on the Stardust aluminum foils. *Meteorit. Planet. Sci.* **43**, 41–73 (2008). doi: 10.1111/j.1945-5100.2008.tb00609.x
14. D. Brownlee *et al*., Comet 81P/Wild 2 under a microscope. *Science* **314**, 1711–1716 (2006). doi: 10.1126/science.1135840; pmid: 17170289
15. M. Zolensky *et al*., Comparing Wild 2 particles to chondrites and IDPs. *Meteorit. Planet. Sci.* **43**, 261–272 (2008). doi: 10.1111/j.1945-5100.2008.tb00621.x
16. A. Rotundi *et al*., Two refractory Wild2 terminal particles from a carrot-shaped track characterized combining MIR/FIR/Raman micro-spectroscopy and FE-SEM/EDS analyses. *Meteorit. Planet. Sci.* **49**, 550–575 (2014).
17. S. Gulkis *et al*., Subsurface properties and early activity of comet Churyumov-Gerasemenko. *Science* **347**, aaa0709 (2015). doi: 10.1126/science.aaa0709
18. M. Fulle *et al*., Comet 67P/Churyumov-Gerasimenko: The GIADA dust environment model of the Rosetta mission target. *Astron. Astrophys.* **522**, A63–A80 (2010). doi: 10.1051/0004-6361/201014928
19. M. Fulle, Injection of large grains into orbits around comet nuclei. *Astron. Astrophys.* **325**, 1237–1248 (1997).
20. K. Richter, H. U. Keller, On the stability of dust particle orbits around cometary nuclei. *Icarus* **114**, 355–371 (1995). doi: 10.1006/icar.1995.1068
21. D. J. Scheeres, F. Marzari, Temporary orbital capture of ejecta from comets and asteroids: Application to the Deep Impact experiment. *Astron. Astrophys.* **356**, 747–756 (2000).
22. C. Snodgrass *et al*., Beginning of activity in 67P/Churyumov-Gerasimenko and predictions for 2014-2015. *Astron. Astrophys.* **557**, A33 (2013). doi: 10.1051/0004-6361/201322020
23. J. Agarwal *et al*., The dust trail of comet 67P/Churyumov-Gerasimenko between 2004 and 2006. *Icarus* **207**, 992–1012 (2010). doi: 10.1016/j.icarus.2010.01.003
24. J. F. Crifo, G. A. Lukyanov, V. V. Zakharov, A. V. Rodionov, "Physical model of the coma of Comet 67P/Churyumov–Gerasimenko," in *The New Rosetta Targets. Observations, Simulations and Instrument Performances*, L. Colangeli, E. Mazzotta Epifani, P. Palumbo, Eds. (Kluwer Academic, Dordrecht, 2004), pp. 119–131.
25. M. Hässig *et al*., Time variability and heterogeneity in the coma of 67P/Churyumov-Gerasimenko. *Science* **347**, aaa0276 (2015). doi: 10.1126/science.aaa0276

ACKNOWLEDGMENTS

GIADA was built by a consortium led by the Università degli Studi di Napoli "Parthenope" and INAF—Osservatorio Astronomico di Capodimonte, in collaboration with the Instituto de Astrofisica de Andalucia, Selex-ES, FI, and SENER. GIADA is presently managed and operated by Istituto di Astrofisica e Planetologia Spaziali–INAF, Italy. GIADA was funded and managed by the Agenzia Spaziale Italiana, with the support of the Spanish Ministry of Education and Science Ministerio de Educacion y Ciencias (MEC). GIADA was developed from a Principal Investigator proposal from the University of Kent; science and technology contributions were provided by CISAS, Italy; Laboratoire d'Astrophysique Spatiale, France, and institutions from the UK, Italy, France, Germany, and the USA. Science support was provided by NASA through the U.S. Rosetta Project managed by the Jet Propulsion Laboratory/California Institute of Technology. We would like to thank A. Coradini for her contribution as a GIADA Co-Investigator. GIADA calibrated data will be available through ESA's Planetary Science Archive (PSA) Web site (www.rssd.esa.int/index.php?project=PSA&page=index). All data presented here are available on request before archival in the PSA. OSIRIS was built by a consortium led by the Max-Planck-Institut für Sonnensystemforschung, Katlenburg-Lindau, Germany, in collaboration with CISAS, University of Padova, Italy; the Laboratoire d'Astrophysique de Marseille, France; the Instituto de Astrofísica de Andalucia, CSIC, Granada, Spain; the Scientific Support Office of the European Space Agency, Noordwijk, The Netherlands; the Instituto Nacional de Técnica Aeroespacial, Madrid, Spain; the Universidad Politéchnica de Madrid, Spain; the Department of Physics and Astronomy of Uppsala University, Sweden; and the Institut für Datentechnik und Kommunikationsnetze der Technischen Universität Braunschweig, Germany. The support of the national funding agencies of Germany (DLR), France (Centre National d'Etudes Spatiales), Italy (Italian Space Agency), Spain (MEC), Sweden (Sweden National Science Board), and the ESA Technical Directorate is gratefully acknowledged. We thank the MIRO and ROSINA teams for sharing their early results with us. We thank the Rosetta Science Ground Segment at ESAC, the Rosetta Mission Operations Centre at ESOC (European Space Operations Center), and the Rosetta Project at ESTEC (European Space Technology Center) for their outstanding work enabling the science return of the Rosetta Mission. We gratefully acknowledge the referees for very constructive comments.

SUPPLEMENTARY MATERIALS

www.sciencemag.org/content/347/6220/aaa3905/suppl/DC1
Supplementary Text
Fig. S1
Tables S1 to S3
References

29 November 2014; accepted 1 January 2015
10.1126/science.aaa3905